Magnetic ground state of CrOCl: A first-principles study

Haoran Zhu,[1] Peixuan Liu,[1] Xu Zuo,[1,2,3,*] and Bin Shao[1,4,†]

[1]*College of Electronic Information and Optical Engineering, Nankai University, Tianjin 300350, China*
[2]*Key Laboratory of Photoelectronic Thin Film Devices and Technology of Tianjin, Nankai University, Tianjin 300350, China*
[3]*Engineering Research Center of Thin Film Optoelectronics Technology, Ministry of Education, Nankai University, Tianjin 300350, China*
[4]*Tianjin Key Laboratory of Optoelectronic Sensor and Sensing Network Technology, Nankai University, Tianjin 300350, China*

(Received 6 July 2023; accepted 18 September 2023; published 26 September 2023)

By first-principles calculations, this paper reveals that the antiferromagnetic (AFM) ground state of CrOCl with an orthorhombic structure observed in experiment is mainly due to the competition between the neighboring magnetic exchange interactions (J_i's). The AFM ground state requires that the first and second nearest neighbors (J_1 and J_2) are AFM couplings with comparable magnitudes, and that the seventh nearest neighbor (J_7) has a certain size of AFM coupling. By using Liechtenstein's density functional theory (DFT + U) method and appropriately adjusting the on-site exchange ($\mathcal{J}$) parameter, the J_i's can satisfy these conditions and lead to the experimentally observed AFM ground state (AFM-Exp). The $\mathcal{J}$ parameter changes the energy levels of the Cr-3d orbitals and consequently the energy differences between the orbitals, which in turn impacts the sign and magnitude of J_i's. By decomposing the J_i's into orbital contributions, it is shown that introducing the $\mathcal{J}$ parameter significantly reduces the ferromagnetic parts of J_1 and J_2 and converts them to AFM coupling, which leads to the AFM-Exp ground state.

DOI: 10.1103/PhysRevB.108.094435

I. INTRODUCTION

Magnetic materials have received widespread attention for a long time due to their potential applications in spintronics, magnetic storage devices, logic circuits, and sensors [1–5]. The recent discovery of $Cr_2Ge_2Te_6$ and CrI_3 ferromagnetic monolayers [6,7] provided opportunities for the development of two-dimensional (2D) spintronic devices that offer ultralow-energy consumption, ultrafast device operation, and ultrahigh-density information storage [8–10].

Recently, a series of theoretical calculations [11–16] predicted that the CrOCl monolayer is a ferromagnetic (FM) 2D material with a high Curie temperature (T_C), and CrOCl bulk is an A-type antiferromagnetic (AFM) material with an interlayer AFM exchange interaction and intralayer FM exchange interaction. However, early and recent experiments [17–20] show that the few-layer CrOCl is characterized by an intralayer AFM ground state, which has a complicated AFM spin order along the b axis (↑↑↓↓) and quasi-1D FM chains along the a axis. The contradiction between the theoretical calculations and the experimental results prompts us to explore the origin of the AFM ground state of CrOCl by a fine tuning of density functional theory (DFT)-based first-principles calculations.

Generally, magnetic insulators exhibit two types of exchange interactions, including the kinetic exchange (i.e., so-called superexchange) and the direct exchange (always FM and weak) [21]. The semiempirical Goodenough-Kanamori-Anderson (GKA) rules [21–23] were proposed to qualitatively understand the superexchange interactions. However, the crystal field of Cr ions in CrOCl is characterized of a symmetry much lower than octahedral coordination, which leads to more exchange channels or orbital contributions competing with each other. It is therefore crucial to analyze all possible exchange channels to determine the magnetic interactions in this system.

In this paper, we investigate the magnetic ground state and exchange interaction of the CrOCl bulk and monolayer by adopting the rotationally invariant DFT + U introduced by Liechtenstein. We show that the on-site exchange parameter ($\mathcal{J}$) is indispensable to reproduce the AFM ground state of CrOCl bulk measured in experiment, because it will influence the neighboring magnetic exchange interactions. By decomposing the exchange interaction into the orbital contributions, it is shown that the $\mathcal{J}$ parameter weakens the calculated FM coupling parts, making the AFM coupling parts dominant in J_1 and J_2. In addition, the competition between the AFM couplings of the neighbors results in the experimentally observed AFM ground state.

II. COMPUTATIONAL DETAILS

Spin-polarized first-principles calculations based on the projector augmented-wave (PAW) pseudopotentials [24] are implemented in the Vienna *ab initio* simulation package (VASP) [25,26]. The generalized gradient approximation (GGA) in the Perdew-Burke-Ernzerhof form [27,28] is selected as the exchange-correlation functional, following electrons being treated as valence states: Cr-3d and 4s, Cl-2s and 2p, and O-2s and 2p. The DFT + U method is employed

*xzuo@nankai.edu.cn
†bshao@nankai.edu.cn

 ©2023 American Physical Society

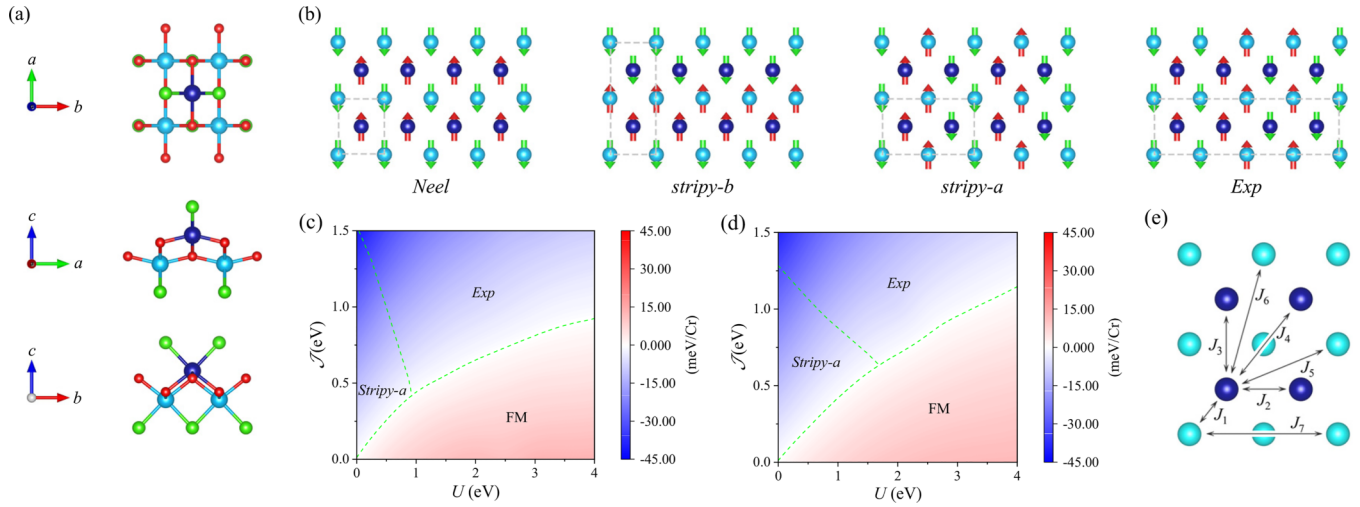

FIG. 1. (a) A top and side view of the CrOCl crystal structure. (b) Four AFM spin orders are considered. Blue, cyan, red, and green spheres represent the Cr atom in the upper sublayer, Cr atom in the lower sublayer, O atom, and Cl atom, respectively. The first-principles phase diagrams of the CrOCl (c) bulk and (d) monolayer, where the green dashed lines are phase boundaries. (e) Magnetic exchange paths.

to properly describe the strong electron correlation effect of the Cr-3d orbitals, implemented by the Liechtenstein's approach [29] and Dudarev's approach [30]. A cutoff energy of 500 eV is used for the plane-wave expansion. The convergence criteria of structure optimization are 10^{-5} eV and 0.01 eV Å^{-1} for energy and force, respectively. To isolate the interactions from the periodic images, a vacuum space of 20 Å is included. A Monkhorst-Pack k-point mesh of $10 \times 8 \times 1$ ($10 \times 2 \times 1$) is utilized in the structural optimizations and the calculations of the electronic and magnetic properties for the $1 \times 1 \times 1$ ($1 \times 4 \times 1$) unit cells. In addition, explicit energy dispersion correction terms are employed by using the DFT-D3 method [31,32]. The phonon dispersion is calculated using a $3 \times 4 \times 1$ supercell with the finite displacement method by the PHONOPY software [33,34]. The exchange interactions are calculated by using the four-state method [35] with $4 \times 5 \times 1$ supercells and the Green's function method based on magnetic force theory by using the TB2J code [36]. In the latter method, the exchange integral is calculated by

$$J_{ij} = -\frac{1}{4}\int_{-\infty}^{E_F} \mathrm{Im\,Tr}\{\Delta_{im} G^{\uparrow}_{im,jn} \Delta_{jn} G^{\downarrow}_{jn,im}\} d\varepsilon, \qquad (1)$$

where (i, j) and (m, n) denote the site and local orbital indices, respectively, $G^{\uparrow}_{im,jn}$ is the intersite Green's function, Δ_{im} ($\Delta_{im} = H^{\uparrow}_{im} - H^{\downarrow}_{im}$) is the energy differences between spin-up and spin-down orbitals, Tr denotes the trace over the orbital indices, and E_F is the Fermi energy. The Green's function can be derived from the Wannier functions (WFs), which can be reconstructed from the wave functions by the first-principles calculation (the VASP code in this work) by using the WANNIER90 code [37,38].

III. RESULTS AND DISCUSSION

A. Magnetic ground state

The orthorhombic chromium oxyhalide CrOCl bulk with the space group *Pmmn* [17] is a layered van der Waals (vdW) AFM semiconductor. Figure 1(a) shows that each Cr atom is coordinated by four oxygen atoms and two halogen atoms, forming a distorted octahedron of CrO_4Cl_2. Several previous theoretical studies [11–16] predicted the CrOCl monolayer is an FM semiconductor, but experimental studies [17–20] showed that the CrOCl bulk is an AFM semiconductor, with intralayer AFM spin order, the magnetic ground-state structure is shown in Fig. 1(b) and named AFM-Exp. To investigate the discrepancy between experimental results and theoretical predictions, we compare the effects of the on-site Coulomb parameter (U) and on-site exchange parameter ($\mathcal{J}$) on the magnetic ground state of CrOCl bulk using the Dudarev's approach and Liechtenstein's approach of the DFT + U method. In the Dudarev's approach, only the effective U_{eff} ($U_{\mathrm{eff}} = U - \mathcal{J}$) is significant, which is equivalent to $\mathcal{J} = 0$ eV in the Liechtenstein's approach.

To investigate the magnetic ground state of both CrOCl bulk and monolayer at different U and $\mathcal{J}$ parameters, we calculate the total energies of one FM state and four AFM states. The AFM states are shown in Fig. 1(b). By comparing the total energies, it is shown that the FM state is the magnetic ground state for CrOCl bulk and monolayer within a wide range of the U values when $\mathcal{J} = 0$ eV, as shown in Figs. 1(c) and 1(d). This result is consistent with previous predictions for CrOCl monolayer [11–16]. However, the CrOCl bulk is also predicted to be FM, which is inconsistent with the experimental result, indicating that the accuracy of previous calculations is questionable.

Figures 1(c) and 1(d) highlight that the $\mathcal{J}$ parameter is indispensable in determining the magnetic ground state of CrOCl bulk. In addition, we also calculate the effects of the U and $\mathcal{J}$ parameters on the interlayer magnetic coupling of the CrOCl bulk. As shown in Supplemental Fig. S1 [39], without considering the $\mathcal{J}$ parameter, the interlayer magnetic coupling is FM, suggesting that it is not possible to form an A-type AFM structure [12] (intralayer FM coupling and interlayer AFM coupling). In addition, the interlayer magnetic coupling is about two orders of magnitude weaker than

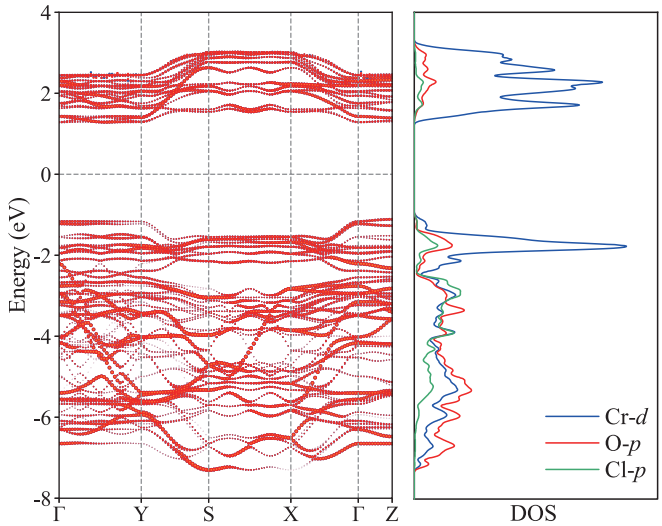

FIG. 2. Electronic band structure and projected density of states (PDOS) of CrOCl bulk. Since the CrOCl bulk is an AFM-Exp structure, the spin-up and spin-down bands are identical and the PDOS only shows the spin-up part.

the intralayer magnetic coupling, indicating their negligible impact on the intralayer spin order. The above results show that the $\mathcal{J}$ parameter plays an extremely important role in describing the AFM ground state of CrOCl. Therefore, we focus on the specific effect of the $\mathcal{J}$ parameter on the magnetic couplings and fix the U parameter to a value of 3 eV, since the calculated band gap of the system (∼2.39 eV, shown in Fig. 2) is consistent with the experimental values [17–20] when $U = 3$ eV and $\mathcal{J} = 1.5$ eV. Also, from the density of states (DOS) in Fig. 2, it can be observed that the valence band maximum (VBM) and conduction band minimum (CBM) of CrOCl bulk are mainly contributed by Cr-3d orbitals and the 2p orbital energy levels of the anion are lower than the Cr-3d orbitals, indicating the distribution of energy levels is critical for the magnetic exchange channel.

B. Competition between magnetic exchange interactions

To investigate the origin of the AFM ground state (AFM-Exp) of CrOCl, we analyze the competition between exchange interactions and its influence on the magnetic ground of the system. Using the four-state (FS) method and magnetic force (MF) theory, we calculate the magnetic exchange interactions of the first seven nearest neighbors, as shown in Fig. 1(e). As listed in Table I, J_i's obtained from the MF theory are consistent with those from the FS method, where the values of J_4, J_5, and J_6 are small enough to be neglected. In addition, J_3 is very small from the result of $\mathcal{J} = 1.5$ eV, but the AFM-Exp structure can still be obtained, indicating that the effect of J_3 on the AFM-Exp structure is negligible. The magnetic ground state is determined by J_1, J_2, and J_7. With a $\mathcal{J}$ parameter of 0 eV, J_1 and J_2 are FM couplings, and with a $\mathcal{J}$ parameter of 1.5 eV, J_1 and J_2 are AFM couplings. In AFM-Exp spin order, the spin direction between all Cr atoms and their seventh nearest neighbor's Cr atoms is opposite, hinting that an AFM J_7 is indispensable. Therefore, the Heisenberg model involving J_1, J_2, and J_7 is considered to calculate the magnetic phase diagram of CrOCl:

TABLE I. The calculated magnetic exchange interaction parameters J_i (in meV) for CrOCl by the four-state (FS) method and magnetic force (MF) theory with $U = 3$ eV and $\mathcal{J} = 0$ and 1.5 eV. The J_i's are defined in Fig. 1(e).

	$\mathcal{J} = 0$ eV		$\mathcal{J} = 1.5$ eV	
	FS	MF	FS	MF
J_1	1.44	1.69	−1.05	−1.41
J_2	0.99	0.85	−0.98	−1.54
J_3	5.00	5.79	0.04	0.09
J_4	0.05	0.00	0.07	−0.02
J_5	0.03	0.01	0.02	0.00
J_6	0.06	0.04	−0.06	−0.06
J_7	−0.31	−0.20	−0.28	−0.22

$$H = -\sum_{\langle ij\rangle} J_1 \vec{S}_i \cdot \vec{S}_j - \sum_{\langle\langle ij\rangle\rangle} J_2 \vec{S}_i \cdot \vec{S}_j - \sum_{\langle\langle\langle ij\rangle\rangle\rangle} J_7 \vec{S}_i \cdot \vec{S}_j. \quad (2)$$

As shown in Fig. 3(a), when only J_1 and J_2 are considered, in spite of their magnitude and sign, there is no AFM-Exp in the magnetic phase diagram. In addition, when the FM J_3 is included, the magnetic phase diagram as shown in Supplemental Fig. S4(a) [39] is the same as that in Fig. 3(a), which confirms that J_3 might not lead to the AFM-Exp phase and it can be ignored. However, when the AFM J_7 is included in the Heisenberg model in Eq. (2), there is an AFM-Exp phase as shown in Fig. 3(b). In addition, the phase diagram shows that two conditions must be satisfied for the emergence of AFM-Exp spin order: (a) J_1 and J_2 must be AFM coupling and have a comparable magnitude; (b) J_7 must be AFM coupling [the phase diagram for a FM J_7 is shown in Supplemental Fig. S4(b) [39], indicating that there is no AFM-Exp spin order]. We also examine the influence of lattice distortion in this study, as detailed in Sec. II of the Supplemental Material [39].

When the $\mathcal{J}$ parameter is 0 eV, the exchange interactions calculated by using the FS method and MF theory fall into the FM region of the phase diagram, represented by the black circle and triangle in Fig. 3(b). However, when the $\mathcal{J}$ parameter of 1.5 eV, they fall into the AFM-Exp region, represented by the green circle and triangle in Fig. 3(b). This suggest that the $\mathcal{J}$ parameter plays a crucial role in determining the intralayer spin order of the CrOCl.

To gain a better understanding of the effect of $\mathcal{J}$ parameter on J_i's, we used the Green's function method to calculate the orbital-resolved J_i's, which allow us to reveal the microscopic magnetic exchange mechanism of CrOCl. In an octahedral crystal field, the fivefold degenerate 3d orbitals of Cr will split into two groups: t_{2g} orbitals (d_{xy}, d_{xz}, and d_{yz}) and e_g ($d_{x^2\text{-}y^2}$ and d_{z^2}). Because the octahedron of CrO_4Cl_2 is distorted and there are two Cl atoms, the degeneracy of 3d orbitals will be further lifted. The t_{2g} orbitals will be split into a singlet state b_2 (d_{xy}) and a doublet state e (d_{xz}, d_{yz}), and e_g orbitals will be split into two singlet states b_1 ($d_{x^2\text{-}y^2}$) and a_1 (d_{z^2}), as shown in Fig. 4. The three d electrons of Cr^{3+} occupy b_2 and e orbitals, giving rise to local magnetic moments of $3\mu_B$.

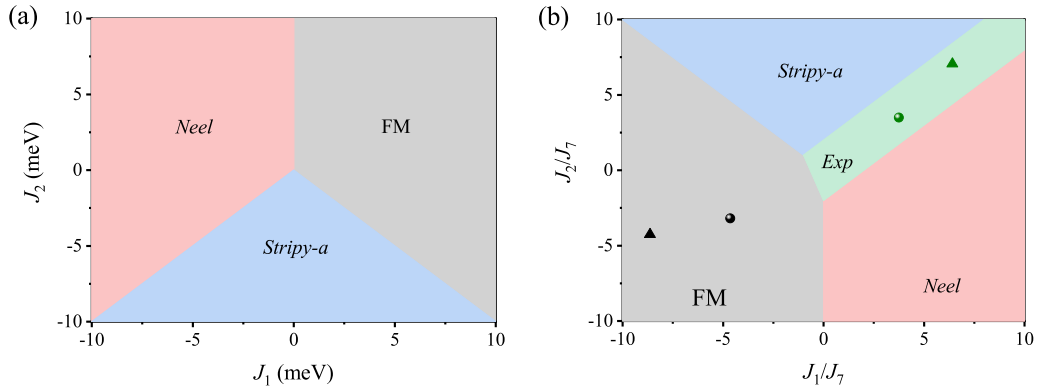

FIG. 3. The magnetic phase diagram of the Heisenberg model (2) in the text as a function of (a) J_1 and J_2, and (b) J_1/J_7 and J_2/J_7. Since our calculation shows that J_7 is AFM, only $J_7 < 0$ is considered. The black circle and triangle represent the points calculated by the FS method and MF theory, respectively, at $U = 3$ eV and $\mathcal{J} = 0$ eV, and the green circle and triangle represent the points calculated by the FS method and MF theory, respectively, at $U = 3$ eV and $\mathcal{J} = 1.5$ eV.

From the orbital-resolved J_i's shown in Fig. 5, J_1 originates mainly from the e-e, b_2-e, and e-a_1 hopping channels [Figs. 5(a) and 5(d)], J_2 is primarily from the e-e, b_2-b_2, and b_2-b_1 hopping channels [Figs. 5(b) and 5(e)], while J_7 is primarily from the b_2-b_2 hopping channel [Figs. 5(c) and 5(f)]. The contributions of other hopping channels are relatively weak, due to the local structure. For J_1, as shown in Figs. 6(a)–6(c), the e-e direct hopping induces AFM coupling [Fig. 6(a)], and the b_2-e hopping via the b_2-$p_x(p_y)$-e channel also induces AFM coupling [Fig. 6(b)]. In contrast, the e-a_1 hopping via the e-p_z-a_1 channel leads to FM coupling [Fig. 6(c)]. The diagram of the major hopping channels contributing to the J_1 is shown in Supplemental Figs. S5(a) and S5(b) [39]. As for J_2, the b_2-b_2 direct hopping generates AFM coupling [Fig. 6(d)], and the e-e hopping via the e-p_z-e channel generates AFM coupling [Fig. 6(e)]. Conversely, the b_2-b_1 hopping via the b_2-$p_x(p_y)$-b_1 channel leads to FM coupling [Fig. 6(f)]. The diagram of the major hopping channels contributing to the J_2 is shown in Supplemental Figs. S5(c) and S5(d) [39]. As for J_7, the b_2-b_2 hopping is mainly attributed to two consecutive b_2-b_2 direct hoppings, producing AFM coupling. In the preceding phase diagrams, we also observed that despite the FM J_3 not affecting the magnetic ground state of the system, the magnitude of this coefficient decreases dramatically with the $\mathcal{J}$ parameter; this part is discussed in detail in Sec. II of the Supplemental Material [39].

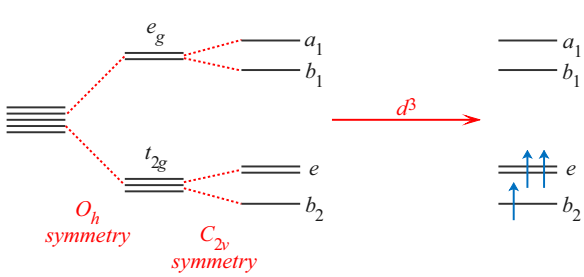

FIG. 4. The $3d$ orbital splitting from an ideal octahedron with O_h symmetry to a distorted octahedron with C_{2v} symmetry, and d^3 electrons occupying b_2 and e orbitals.

The dominant contributions to the exchange interactions in CrOCl originate from different hopping channels, demonstrating an essentially different character. According to the well-known Kugel-Khomskii formalism developed on the basis of the superexchange theory [40–42], the total exchange interaction of a multiorbital electronic system can be presented as a sum of all contributions in the following form,

$$J_1 = J_1^{e\text{-}e} + J_1^{e\text{-}b_2} + J_1^{e\text{-}a_1} = -\frac{\left(t_1^{e\text{-}e}\right)^2}{U_{\mathrm{Cr}}} - \frac{4\left(t_1^{e\text{-}b_2}\right)^2}{\Delta_{e\text{-}b_2}} + \frac{4\left(t_1^{e\text{-}a_1}\right)^2 \mathcal{J}_H}{\Delta_{e\text{-}a_1}(\Delta_{e\text{-}a_1} - \mathcal{J}_H)}, \quad (3)$$

$$J_2 = J_2^{b_2\text{-}b_2} + J_2^{e\text{-}e} + J_2^{b_2\text{-}b_1} = -\frac{4\left(t_2^{b_2\text{-}b_2}\right)^2}{U_{\mathrm{Cr}}} - \frac{4\left(t_2^{e\text{-}e}\right)^2}{U_{\mathrm{Cr}}} + \frac{4\left(t_2^{b_2\text{-}b_1}\right)^2 \mathcal{J}_H}{\Delta_{b_2\text{-}b_1}(\Delta_{b_2\text{-}b_1} - \mathcal{J}_H)}, \quad (4)$$

where t, U_{Cr} ($U_{\mathrm{Cr}} = \varepsilon_{d\uparrow}^{\mathrm{occupy}} - \varepsilon_{d\downarrow}^{\mathrm{unoccupy}}$), Δ, and $\mathcal{J}_H$ in Eqs. (3) and (4) are the effective hoppings between the orbitals on two Cr atoms, the strength of the exchange split, the energy differences between two Cr-d orbitals, and the Hund's coupling of d electrons, respectively. Here, the first terms of Eqs. (3) and (4) are associated with the direct hoppings of an electron from the occupied orbital of one Cr atom to the empty orbital of another Cr atom [Figs. 6(a) and 6(d)]. The second terms are the AFM superexchange interactions mediated by the p orbitals of the ligands [Figs. 6(b) and 6(e)]. The third term refers to the FM superexchange interaction involving the intra-atomic exchange $\mathcal{J}_H$ [Figs. 6(c) and 6(f)], which is related to the spin splitting of the empty a_1 orbital (or the empty b_1 orbital) [43]. As shown in Supplemental Figs. S8(a) and S8(b) [39], the spin splitting is significantly reduced by the inclusion of the $\mathcal{J}$ parameter, suggesting a possible reduction of $\mathcal{J}_H$ (the smaller the value of $\mathcal{J}_H$, the weaker is the FM coupling) [44]. Since the last two terms of Eqs. (3) and (4) involve p-d covalency, t depends on the energy difference between the p-d orbitals ($\Delta_{p\text{-}d}$), where the smaller is $\Delta_{p\text{-}d}$, the larger is t [45]. The corresponding parameters of U_{Cr} and Δ's can be extracted by projecting the Kohn-Sham states on the atomic Wannier

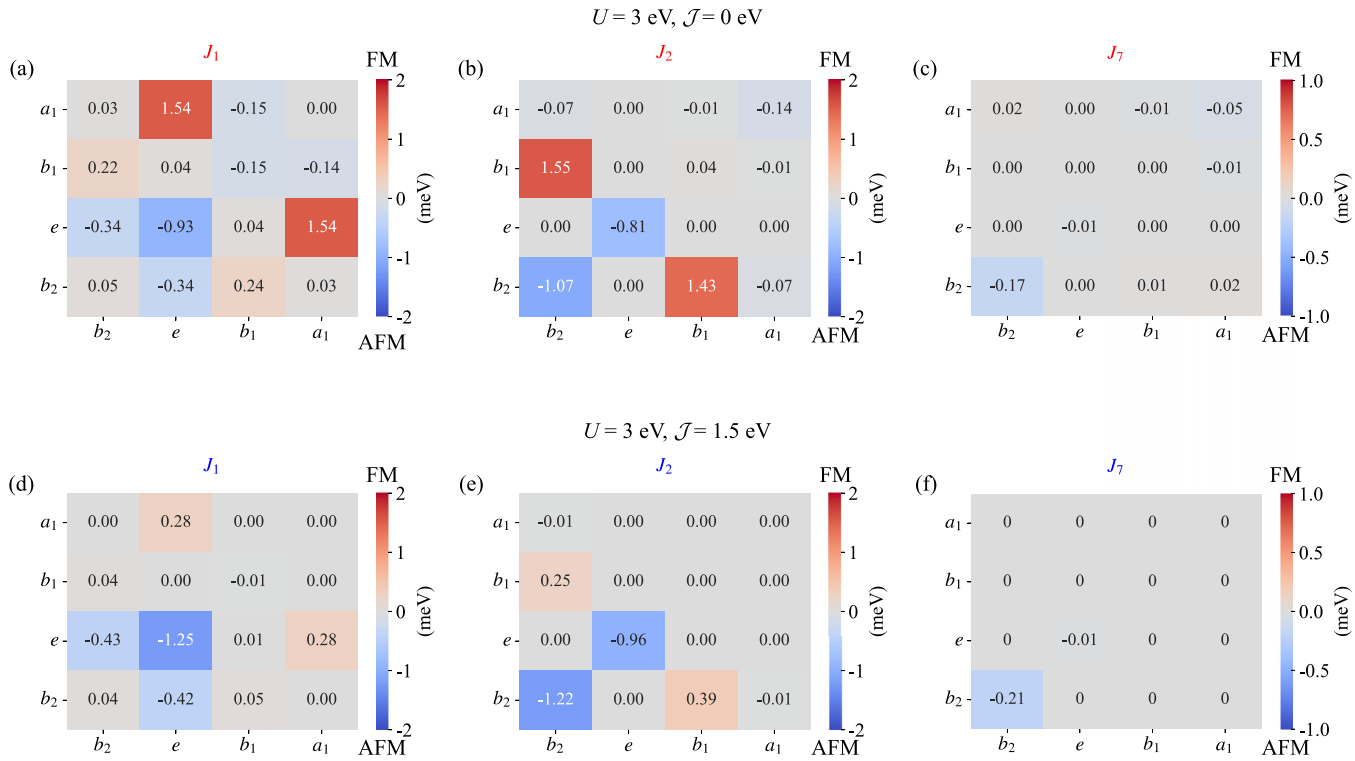

FIG. 5. For $U = 3$ eV and $\mathcal{J} = 0$ eV, the decomposition of (a) J_1, (b) J_2, and (c) J_7 to the contributions of different $3d$ orbitals in CrOCl. Similarly, (d)–(f) are the orbital decompositions of J_1, J_2, and J_7, respectively, with $U = 3$ eV and $\mathcal{J} = 1.5$ eV as the parameters.

functions of Cr-3d, O-2p, and Cl-2p orbitals, as shown in Table II.

The decrease in energy of the spin splitting of the empty a_1 orbital (or the empty b_1 orbital) is related to the double counting of the exchange interaction in the DFT + U formalism and the exchange interaction in the GGA. According to the double counting energy outlined in the original literature of the DFT + U method [29],

$$E_{\mathrm{DC}}[\{n^\sigma\}] = \tfrac{1}{2}Un(n-1) - \tfrac{1}{2}\mathcal{J}[n^\uparrow(n^\uparrow - 1) + n^\downarrow(n^\downarrow - 1)], \tag{5}$$

we can observe that the potential of the double counting correction term is spin dependent:

$$V_{\mathrm{DC}}^\sigma = U\left(n - \tfrac{1}{2}\right) - \mathcal{J}\left(n^\sigma - \tfrac{1}{2}\right). \tag{6}$$

For the CrOCl system, the b_2 and e orbitals are half filled, while the a_1 and b_1 orbitals are empty, i.e., the system has three electrons with spin-up. Therefore, the potential energy difference of the spin splitting in the a_1/b_1 orbitals is as follows,

$$\begin{aligned}\Delta V_{a_1/b_1} &= |V_{a_1/b_1}^\downarrow - V_{\mathrm{DC}}^\downarrow - (V_{a_1/b_1}^\uparrow - V_{\mathrm{DC}}^\uparrow)| \\ &= |V_{a_1/b_1}^\downarrow - V_{a_1/b_1}^\uparrow - 3\mathcal{J}|,\end{aligned} \tag{7}$$

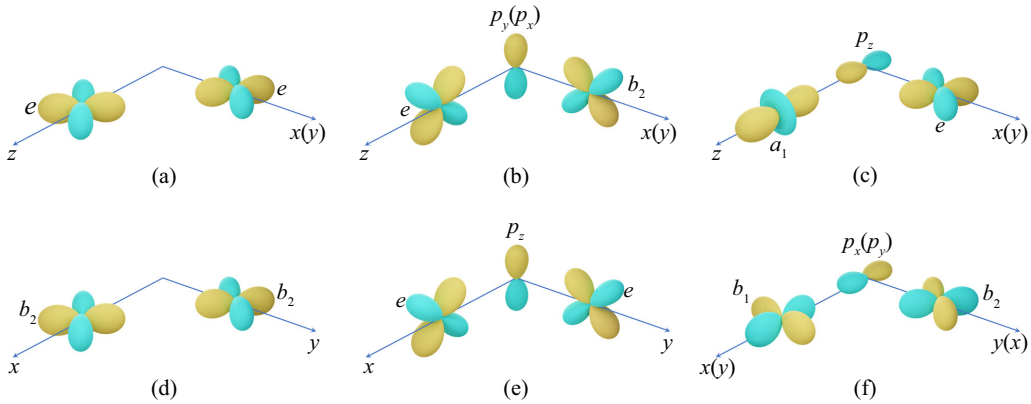

FIG. 6. Hopping channels for J_1: (a) e-e, (b) b_2-e, and (c) e-a_1; J_2: (d) b_2-b_2, (e) e-e, and (f) b_2-b_1. Based on the octahedron of CrO_4Cl_2, the coordinate system of the orbital is defined as follows: $\vec{x} = \frac{1}{\sqrt{2}}(\frac{\vec{b}}{|\vec{b}|} + \frac{\vec{c}}{|\vec{c}|})$, $\vec{y} = \frac{1}{\sqrt{2}}(-\frac{\vec{b}}{|\vec{b}|} + \frac{\vec{c}}{|\vec{c}|})$, $\vec{z} = \frac{\vec{a}}{|\vec{a}|}$.

TABLE II. The strength of exchange field (U_{Cr}, in eV), the differences in energy between Cr-3d orbitals ($\Delta_{e\text{-}b_2}$, $\Delta_{e\text{-}a_1}$, and $\Delta_{b_2\text{-}b_1}$, in eV), and the differences in energy between Cr-3d and O-2p orbitals ($\Delta_{p_x/p_y\text{-}b_2}$, $\Delta_{p_z\text{-}a_1}$, $\Delta_{p_z\text{-}e}$, and $\Delta_{p_x/p_y\text{-}b_1}$, in eV) in fixed $U = 3$ eV and specified $\mathcal{J}$ parameter (the differences in energy between Cr-3d and Cl-2p orbitals are indicated in parentheses in the table below, where only the second nearest neighbor involves Cl atom). I, II, and III correspond to the red, green and blue lines in Supplemental Fig. S5 [39], respectively.

		I	II		III	
	$\mathcal{J}$	U_{Cr}	$\Delta_{e\text{-}b_2}$	$\Delta_{p_x/p_y\text{-}b_2}$	$\Delta_{e\text{-}a_1}$	$\Delta_{p_z\text{-}a_1}$
J_1	0	5.73	5.61	5.66	3.03	4.18
	1.5	5.23	5.08	5.74	3.80	4.65
		I	II		III	
	$\mathcal{J}$	U_{Cr}	U_{Cr}	$\Delta_{p_z\text{-}e}$	$\Delta_{b_2\text{-}b_1}$	$\Delta_{p_x/p_y\text{-}b_1}$
J_2	0	5.73	5.73	6.84 (5.30)	2.85	3.32 (3.10)
	1.5	5.23	5.23	6.32 (5.00)	3.48	4.01 (3.67)

where $V^{\uparrow}_{a_1/b_1}$ and $V^{\downarrow}_{a_1/b_1}$ are the spin-up and spin-down effective single-particle potentials for the a_1/b_1 orbital in the DFT + U method, respectively. Equation (7) suggests that the introduction of the $\mathcal{J}$ may lead to a reduction in the spin splitting of the a_1/b_1 orbitals. Adding $\mathcal{J}$ to the DFT + U method may correct the overestimation of d-orbital exchange splitting of DFT + U. A similar phenomenon has been addressed in other literature [46] as well. By following the Hartree-Fock formalism, it can be derived that the exchange splitting is exactly equal to $3\mathcal{J}_H$ [43], and the effective $\mathcal{J}_H$ can be defined numerically as 1/3 of the exchange splitting read from the calculated DOS.

$J_1^{e\text{-}e}$ is mainly influenced by U_{Cr} [$\varepsilon_e^{\uparrow} - \varepsilon_e^{\downarrow}$, corresponding to the red arrow in Supplemental Fig. S5(a) [39]]. Introducing the $\mathcal{J}$ parameter will decrease the magnitude of U_{Cr}, which increases the AFM coupling ($t_1^{e\text{-}e}$ can be considered almost independent of the $\mathcal{J}$ parameter). $J_1^{e\text{-}b_2}$ depends on $t_1^{e\text{-}b_2}$ [related to $\Delta_{p_x/p_y\text{-}b_2}$, corresponding to the green arrow in Supplemental Fig. S5(a) [39]] and $\Delta_{e\text{-}b_2}$. Introducing the $\mathcal{J}$ parameter will decrease the magnitude of $\Delta_{e\text{-}b_2}$ and slightly increase $\Delta_{p_x/p_y\text{-}b_2}$, which will slightly enhance the AFM coupling. $J_1^{e\text{-}a_1}$ is influenced by $\mathcal{J}_H$, $t_1^{e\text{-}a_1}$ [related to $\Delta_{p_z\text{-}a_1}$, corresponding to the blue arrow in Supplemental Fig. S5(b) [39]], and $\Delta_{e\text{-}a_1}$. Introducing the $\mathcal{J}$ parameter will increase the magnitude of $\Delta_{e\text{-}a_1}$ and $\Delta_{p_z\text{-}a_1}$ while decreasing $\mathcal{J}_H$, which decreases the FM coupling. This eventually converts J_1 from FM coupling to AFM coupling. As for J_2, the $\mathcal{J}$ parameter will decrease the magnitude of U_{Cr} and $\Delta_{p_z\text{-}e}$, and will increase the magnitude of $\Delta_{b_2\text{-}b_1}$ and $\Delta_{p_x/p_y\text{-}b_1}$. A decrease in U_{Cr} will increase the AFM coupling $J_2^{b_2\text{-}b_2}$, and a decrease in U_{Cr} and $\Delta_{p_z\text{-}e}$ (increasing $t_2^{e\text{-}e}$) will increase the AFM coupling $J_2^{e\text{-}e}$; nevertheless, an increase in $\Delta_{b_2\text{-}b_1}$ and $\Delta_{p_x/p_y\text{-}b_1}$ (decreasing $t_2^{b_2\text{-}b_1}$), and a decrease in $\mathcal{J}_H$ will decrease the FM coupling $J_2^{b_2\text{-}b_1}$. These eventually convert the J_2 from FM coupling to AFM coupling. Thus, the condition (a) for the emergence of AFM-Exp spin order to be satisfied. In addition, J_7 is almost independent of the $\mathcal{J}$ parameter, satisfying condition (b).

IV. CONCLUSIONS

The DFT + U method is used to investigate the discrepancy between experimental and theoretical predictions of the magnetic ground state of CrOCl and the exchange interaction in CrOCl. Using the Liechtenstein's method with an appropriate on-site exchange ($\mathcal{J}$) parameter, the experimentally observed AFM ground state (AFM-Exp spin order) is correctly predicted. The emergence of AFM-Exp spin order is attributed to the competition between the exchange interactions of different neighbors (J_i's). The AFM-Exp requires that J_1 and J_2 must be AFM coupled with comparable magnitudes and that J_7 must be AFM coupled according to the calculated phase diagram. Using the orbital-resolved J_i's, we show that introducing the $\mathcal{J}$ parameter considerably reduces the strength of the FM coupling part in J_1 and J_2 by modifying the energy differences between the Cr-3d orbitals. As a result, J_1 and J_2 become AFM coupled with comparable magnitudes, which leads to an AFM-Exp spin order in the CrOCl.

ACKNOWLEDGMENTS

This work was financially supported by MOST (Grant No. 2022YFA1504000), the Tianjin Natural Science Foundation (Grant No. 20JCZDJC00750), the Fundamental Research Funds for the Central Universities, Nankai University (Grants No. 63211107, No. 63201182, No. 63231157, and No. 63221009), and the Science Challenge Project (Grant No. TZ2016003-1-105). The authors thank Yang Li at Beijing Computational Science Research Center for his helpful discussions.

[1] H. Li, S. C. Ruan, and Y. J. Zeng, Adv. Mater. **31**, 1900065 (2019).

[2] L. S. Zhang, J. Zhou, H. Li, L. Shen, and Y. P. Feng, Appl. Phys. Rev. **8**, 021308 (2021).

[3] S. Kumari, D. K. Pradhan, N. R. Pradhan, and P. D. Rack, Emergent Mater. **4**, 827 (2021).

[4] Q. H. Hao, H. W. Dai, M. H. Cai, X. D. Chen, Y. T. Xing, H. J. Chen, T. Y. Zhai, X. Wang, and J. B. Han, Adv. Electron. Mater. **8**, 2200164 (2022).

[5] M. Hossain, B. Qin, B. Li, and X. D. Duan, Nano Today **42**, 101338 (2022).

[6] C. Gong, L. Li, Z. L. Li, H. W. Ji, A. Stern, Y. Xia, T. Cao, W. Bao, C. Z. Wang, Y. Wang, Z. Q. Qiu, R. J. Cava, S. G. Louie, J. Xia, and X. Zhang, Nature (London) **546**, 265 (2017).
[7] B. V. Huang, G. Clark, E. Navarro-Moratalla, D. R. Klein, R. Cheng, K. L. Seyler, D. Zhong, E. Schmidgall, M. A. McGuire, D. H. Cobden, W. Yao, D. Xiao, P. Jarillo-Herrero, and X. D. Xu, Nature (London) **546**, 270 (2017).
[8] S. A. Wolf, D. D. Awschalom, R. A. Buhrman, J. M. Daughton, S. V. Molnár, M. L. Roukes, A. Y. Chtchelkanova, and D. M. Treger, Science **294**, 1488 (2001).
[9] I. Žutić, J. Fabian, and S. D. Sarma, Rev. Mod. Phys. **76**, 323 (2004).
[10] A. Fert, Rev. Mod. Phys. **80**, 1517 (2008).
[11] N. Mounet, M. Gibertini, P. Schwaller, D. Campi, A. Merkys, A. Marrazzo, T. Sohier, I. E. Castelli, A. Cepellotti, G. Pizzi, and N. Marzari, Nat. Nanotechnol. **13**, 246 (2018).
[12] N. H. Miao, B. Xu, L. G. Zhu, J. Zhou, and Z. M. Sun, J. Am. Chem. Soc. **140**, 2417 (2018).
[13] C. Wang, X. Y. Zhou, L. W. Zhou, N. H. Tong, Z. Y. Lu, and W. Ji, Sci. Bull. **64**, 293 (2019).
[14] A. K. Nair, S. Rani, M. V. Kamalakar, and S. J. Ray, Phys. Chem. Chem. Phys. **22**, 12806 (2020).
[15] X. M. Qing, H. Li, C. G. Zhong, P. X. Zhou, Z. C. Dong, and J. M. Liu, Phys. Chem. Chem. Phys. **22**, 17255 (2020).
[16] C. Y. Xu, J. Zhang, Z. X. Guo, S. Q. Zhang, X. X. Yuan, and L. R. Wang, J. Phys.: Condens. Matter **33**, 195804 (2021).
[17] A. N. Christensen, T. Johansson, and S. Quézel, Acta Chem. Scand. **28a**, 1171 (1974).
[18] L. Coïc, M. Spiesser, P. Palvadeau, and J. Rouxel, Mater. Res. Bull. **16**, 229 (1981).
[19] Y. N. Wang, X. Gao, K. N. Yang, P. F. Gu, X. Lu, S. H. Zhang, Y. C. Gao, N. J. Ren, B. J. Dong, Y. H. Jiang, K. Watanabe, T. Taniguchi, J. Kang, W. K. Lou, J. H. Mao, J. P. Liu, Y. Ye, Z. Han, K. Chang, J. Zhang *et al.*, Nat. Nanotechnol. **17**, 1272 (2022).
[20] M. J. Zhang, Q. F. Hu, Y. Q. Huang, C. Q. Hua, M. Cheng, Z. Liu, S. J. Song, F. G. Wang, H. Z. Lu, P. M. He, G. H. Cao, Z. A. Xu, Y. H. Lu, J. B. Yang, and Y. Zheng, Small **19**, 2300964 (2023).
[21] P. W. Anderson, Phys. Rev. **115**, 2 (1959).
[22] J. B. Goodenough, J. Phys. Chem. Solids **6**, 287 (1958).
[23] J. Kanamori, J. Phys. Chem. Solids **10**, 87 (1959).
[24] P. E. Blöchl, Phys. Rev. B **50**, 17953 (1994).
[25] G. Kresse and J. Furthmüller, Phys. Rev. B **54**, 11169 (1996).
[26] G. Kresse and D. Joubert, Phys. Rev. B **59**, 1758 (1999).
[27] J. P. Perdew, J. A. Chevary, S. H. Vosko, K. A. Jackson, M. R. Pederson, D. J. Singh, and C. Fiolhais, Phys. Rev. B **46**, 6671 (1992).
[28] J. P. Perdew and Y. Wang, Phys. Rev. B **45**, 13244 (1992).
[29] A. I. Liechtenstein, V. I. Anisimov, and J. Zaanen, Phys. Rev. B **52**, R5467 (1995).
[30] S. L. Dudarev, G. A. Botton, S. Y. Savrasov, C. J. Humphreys, and A. P. Sutton, Phys. Rev. B **57**, 1505 (1998).
[31] S. Grimme, J. Antony, S. Ehrlich, and H. Krieg, J. Chem. Phys. **132**, 154104 (2010).
[32] S. Grimme, S. Ehrlich, and L. Goerigk, J. Comput. Chem. **32**, 1456 (2011).
[33] X. Gonze and C. Lee, Phys. Rev. B **55**, 10355 (1997).
[34] A. Togo, F. Oba, and I. Tanaka, Phys. Rev. B **78**, 134106 (2008).
[35] H. J. Xiang, C. Lee, H.-J. Koo, X. G. Gong, and M.-H. Whangbo, Dalton Trans. **42**, 823 (2013).
[36] X. He, N. Helbig, M. J. Verstraete, and E. Bousquet, Comput. Phys. Commun. **264**, 107938 (2021).
[37] A. A. Mostofi, J. R. Yates, Y.-S. Lee, I. Souza, D. Vanderbilt, and N. Marzari, Comput. Phys. Commun. **178**, 685 (2008).
[38] G. Pizzi, V. Vitale, R. Arita, S. Blügel, F. Freimuth, G. Géranton, M. Gibertini, D. Gresch, C. Johnson, T. Koretsune, J. Ibañez-Azpiroz, H. Lee, J.-M. Lihm, D. Marchand, A. Marrazzo, Y. Mokrousov, J. I. Mustafa, Y. Nohara, Y. Nomura, L. Paulatto *et al.*, J. Phys.: Condens. Matter **32**, 165902 (2020).
[39] See Supplemental Material at http://link.aps.org/supplemental/10.1103/PhysRevB.108.094435 for the supplemental material provides more information elucidating the underlying factors contributing to the magnetic ground state of CrOCl.
[40] K. I. Kugel' and D. I. Khomskii, Zh. Eksp. Teor. Fiz. **64**, 1429 (1973) [Sov. Phys. JETP **37**, 725 (1973)].
[41] K. I. Kugel' and D. I. Khomskii, Sov. Phys. Usp. **25**, 231 (1982).
[42] V. V. Mazurenko, F. Mila, and V. I. Anisimov, Phys. Rev. B **73**, 014418 (2006).
[43] M. D. Towler, N. L. Allan, N. M. Harrison, V. R. Saunders, W. C. Mackrodt, and E. Aprà, Phys. Rev. B **50**, 5041 (1994).
[44] I. V. Kashin, V. V. Mazurenko, M. I. Katsnelson, and A. N. Rudenko, 2D Mater. **7**, 025036 (2020).
[45] C. X. Huang, J. S. Feng, F. Wu, D. Ahmed, B. Huang, H. J. Xiang, K. M. Deng, and E. J. Kan, J. Am. Chem. Soc. **140**, 11519 (2018).
[46] H. H. Chen and A. J. Millis, Phys. Rev. B **93**, 045133 (2016).